AGU PUBLICATIONS

JGR

Journal of Geophysical Research: Solid Earth

RESEARCH ARTICLE
10.1002/2016JB013139

Key Points:
- Seismic refraction and reflection data constrain crustal and upper mantle structure of the Salton Trough
- Actively extending crust is 17–18 km thick and roughly one-dimensional for >100 km in the plate motion direction
- North American lithosphere in the central Salton Trough has been rifted apart and is being replaced by new crust

Correspondence to:
L. Han,
lianghan@vt.edu

Citation:
Han, L., et al. (2016), Continental rupture and the creation of new crust in the Salton Trough rift, Southern California and northern Mexico: Results from the Salton Seismic Imaging Project, *J. Geophys. Res. Solid Earth*, *121*, 7469–7489, doi:10.1002/2016JB013139.

Received 2 MAY 2016
Accepted 8 OCT 2016
Accepted article online 11 OCT 2016
Published online 30 OCT 2016

Continental rupture and the creation of new crust in the Salton Trough rift, Southern California and northern Mexico: Results from the Salton Seismic Imaging Project

Liang Han[1], John A. Hole[1], Joann M. Stock[2], Gary S. Fuis[3], Annie Kell[4], Neal W. Driscoll[5], Graham M. Kent[4], Alistair J. Harding[5], Michael J. Rymer[3], Antonio González-Fernández[6], and Octavio Lázaro-Mancilla[7]

[1]Department of Geosciences, Virginia Polytechnic Institute and State University, Blacksburg, Virginia, USA, [2]Seismological Laboratory, California Institute of Technology, Pasadena, California, USA, [3]U.S. Geological Survey, Menlo Park, California, USA, [4]Nevada Seismological Laboratory, University of Nevada, Reno, Reno, Nevada, USA, [5]Scripps Institution of Oceanography, University of California, San Diego, La Jolla, California, USA, [6]Department of Geology, Centro de Investigacion Cientifica y de Educacion Superior de Ensenada, Ensenada, Mexico, [7]Instituto de Ingeniería, Universidad Autónoma de Baja California, Mexicali, Mexico

Abstract A refraction and wide-angle reflection seismic profile along the axis of the Salton Trough, California and Mexico, was analyzed to constrain crustal and upper mantle seismic velocity structure during active continental rifting. From the northern Salton Sea to the southern Imperial Valley, the crust is 17–18 km thick and approximately one-dimensional. The transition at depth from Colorado River sediment to underlying crystalline rock is gradual and is not a depositional surface. The crystalline rock from ~3 to ~8 km depth is interpreted as sediment metamorphosed by high heat flow. Deeper felsic crystalline rock could be stretched preexisting crust or higher-grade metamorphosed sediment. The lower crust below ~12 km depth is interpreted to be gabbro emplaced by rift-related magmatic intrusion by underplating. Low upper mantle velocity indicates high temperature and partial melting. Under the Coachella Valley, sediment thins to the north and the underlying crystalline rock is interpreted as granitic basement. Mafic rock does not exist at 12–18 km depth as it does to the south, and a weak reflection suggests Moho at ~28 km depth. Structure in adjacent Mexico has slower midcrustal velocity, and rocks with mantle velocity must be much deeper than in the Imperial Valley. Slower velocity and thicker crust in the Coachella and Mexicali valleys define the rift zone between them to be >100 km wide in the direction of plate motion. North American lithosphere in the central Salton Trough has been rifted apart and is being replaced by new crust created by magmatism, sedimentation, and metamorphism.

1. Introduction

Passive continental margins represent the transition from continental rifting to oceanic seafloor spreading. Passive margins are typically classified depending upon the magma volume available from decompression melting of the asthenosphere. Some continental margins are magmatically rich, characterized by transitional crust composed primarily of voluminous igneous rocks [e.g., *White and McKenzie*, 1989; *Holbrook and Kelemen*, 1993]. Other continental margins are magma poor, with exposed serpentinized mantle or highly thinned continental crust at the seafloor [e.g., *Whitmarsh et al.*, 2001; *Hopper et al.*, 2004; *Huismans and Beaumont*, 2014; *Brune et al.*, 2014]. Seismic refraction and reflection imaging of the continental margin is the primary method to differentiate the magma-rich and magma-poor end-members.

A more nuanced view of continental margins considers the formation of new transitional crust through a combination of lithospheric stretching, magmatism, and sedimentation. In the classifications mentioned above, sedimentation is not usually considered as having an important influence on active rift mechanisms. However, numerical modeling suggests that sedimentation reduces the time to localize continental rifting into a narrow rift [*Bialas and Buck*, 2009]. The weight of sediment reduces lateral differences in buoyancy forces, promoting narrow rifting. The creation of new crust by voluminous sedimentation and magmatism probably also plays an important role in rifting processes. The Salton Trough in Southern California and northern Mexico (Figure 1) is an excellent site to study continental rifting processes and the roles of sedimentation and magmatism in the creation of transitional crust.

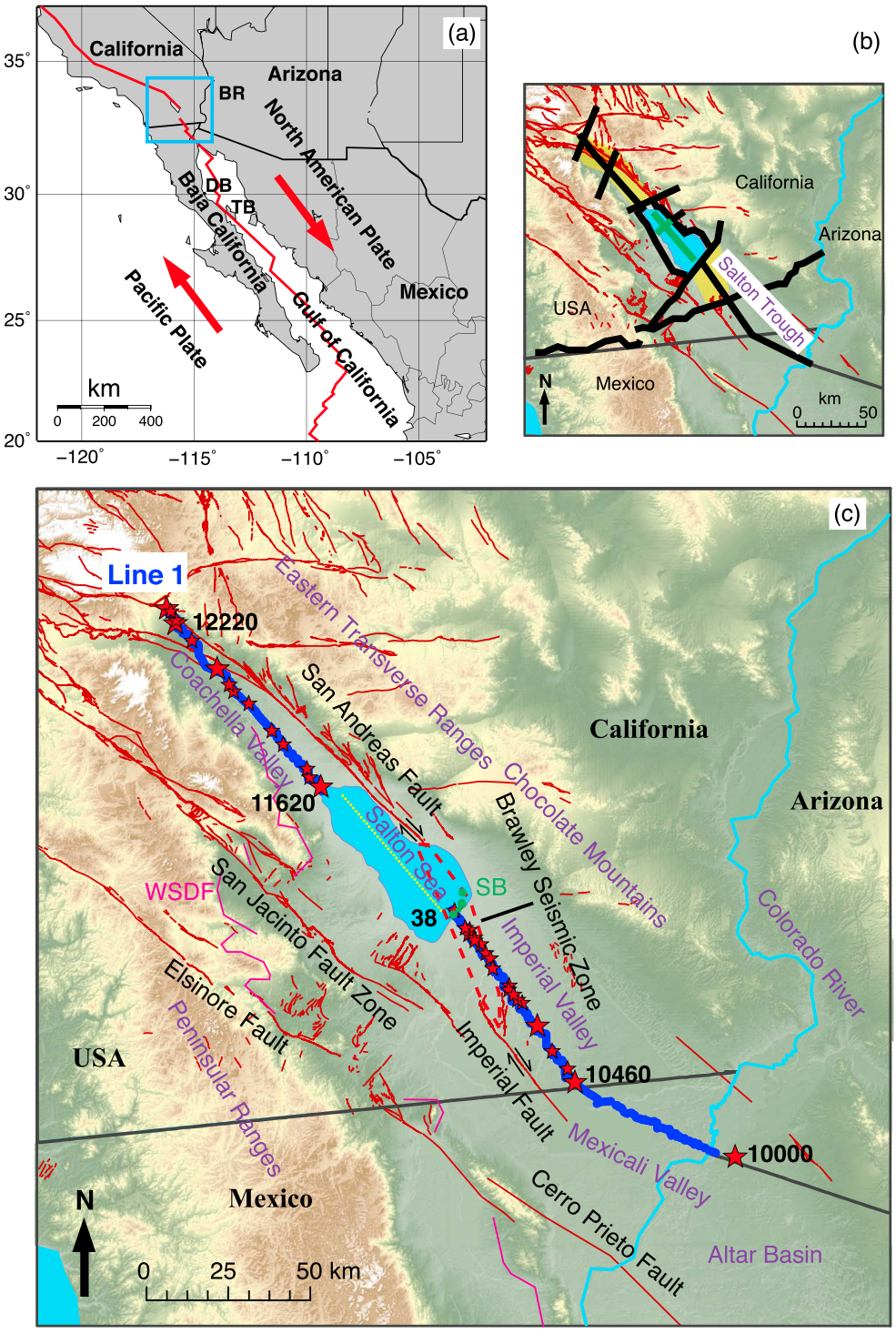

Figure 1. Salton Seismic Imaging Project (SSIP) study area and Line 1 deployment. (a) Rifts and transform faults of the plate boundary in California, Mexico, and the Gulf of California. Arrows show relative motion between Pacific plate and North America plate. Blue box is the survey area in Figures 1b and 1c. BR, Basin and Range; DB, Delfin basin; TB, Tiburon basin. (b) Map of SSIP seismic lines. Thick black lines are onshore 2-D profiles, yellow shaded areas are 3-D grids, and thick green lines in the Salton Sea are OBS arrays. (c) SSIP Line 1 and active faults (red) in the Salton Trough. Red stars are explosive shots, and larger stars correspond to larger shots. Blue dots are onshore seismographs. Yellow dots in the sea are ocean bottom seismographs. Numbered shots and OBS are shown in data Figures 2–6. Green circles at the southeast shore of the Salton Sea are Salton Buttes (SB). The magenta line is the inactive West Salton detachment fault (WSDF) from *Steely et al.* [2009].

The 2011 Salton Seismic Imaging Project (SSIP) was designed to investigate rifting processes at the northern end of the Gulf of California rift system and earthquake hazards at the southern end of the San Andreas Fault system. This paper derives the whole crustal and upper mantle seismic velocity structure along the axis of the Salton Trough, parallel to the direction of relative plate motion, to understand the rifting process. Specific questions include the role of sedimentation on rift localization, whether magmatism from the upper mantle is localized or widely distributed in the lower crust, whether preexisting continental crust underlies the rift, and the extent of rifted crust.

2. Tectonic Setting

The Salton Trough is the northern end of the Gulf of California extensional province (Figure 1) [e.g., *Elders et al*., 1972; *Lonsdale*, 1989; *Stock and Hodges*, 1989; *Larsen and Reilinger*, 1991]. The initial opening of the Gulf of California began about 12 Ma, shortly after subduction ceased along the continental margin of Mexico [*Stock and Hodges*, 1989]. Nearly all of the dextral displacement between the Pacific and North American plates prior to 6.3 Ma was accommodated outside of the Gulf region, and the early rift style was similar to that of the Basin and Range. The entire plate boundary motion was progressively localized into the Gulf of California by ~6 Ma [*Oskin et al*., 2001; *Oskin and Stock*, 2003; *Bennett and Oskin*, 2014].

The Gulf of California is characterized as a series of right-lateral transform faults and relatively short rift segments that result from the plate motion between Pacific Plate and North American Plate (Figure 1). Total opening is estimated to be ~270 km since 6.3 Ma along the entire length of the Gulf of California rift system, including the Salton Trough [*Oskin and Stock*, 2003; *Dorsey et al*., 2007]. In the southern Gulf, the pull-apart rifts have evolved into full seafloor spreading [*Larson et al*., 1968]. In the central Gulf, hundreds of kilometers of oceanic crust are covered by ~4 km thick sediments [*Lizarralde et al*., 2007]. The northern Gulf is underlain by thick sediment from the Colorado River, and the continental crust has been extensively stretched and only recently broken [*Gonzalez-Fernandez et al*., 2005; *Martin-Barajas et al*., 2013].

The Salton Trough is an onshore analog to those rift systems in the Gulf of California, lying at the mouth of the Colorado River (Figure 1). It includes the Coachella Valley, Salton Sea, Imperial Valley, and Mexicali Valley from northwest to southeast. It opens southward toward the Gulf of California and is bounded on the other three sides by mountains of pre-Tertiary igneous and metamorphic rocks [*Elders et al*., 1972]. In addition to an extensional step-over between the right-lateral San Andreas and Imperial Faults (Figure 1), extension has also been accommodated on the west Salton detachment fault [*Axen and Fletcher*, 1998; *Kairouz*, 2005; *Shirvell et al*., 2009]. The Salton Sea is ~70 m below sea level and less than 15 m deep, formed by a drainage canal accident in 1905 that diverted water from the Colorado River, and now evaporation is roughly balanced by irrigation runoff. The Salton Trough and the northern Gulf of California together form the large, low-relief Colorado River delta [*Dorsey*, 2010]. Where the river enters the trough near the U.S.-Mexico border, river sediment isolates the Salton Sea from the ocean in the gulf (Figure 1).

The geometry of these basins is controlled by the faults of the San Andreas Fault system, including the southern San Andreas Fault, the San Jacinto Fault, and the Elsinore Fault (Figure 1). The central part of the Salton Trough was formed by extension between the right-lateral southern San Andreas Fault (SAF) and the Imperial Fault near the Salton Sea and between the Imperial Fault and the Cerro Prieto Fault in northern Mexico (Figure 1). The southern segment of SAF runs along the northeast side of the Salton Trough and terminates at the eastern shore of the Salton Sea. For the past 0.5 Ma, the overall slip is thought to be about equally partitioned between the southern SAF in the Coachella Valley and the parallel northern San Jacinto Fault system [*Janecke et al*., 2010], although slip rates may vary over very short timescales [*Onderdonk et al*., 2015]. Together, these fault systems should add up to most of the ~3.5 cm/yr motion along the Imperial Fault [*Bennett et al*., 1996].

The northern Imperial Valley and southern Salton Sea are seismically highly active. Abundant seismicity occurs at 3–8 km depth in the Salton Sea geothermal field at the southeastern shore of the Salton Sea, 3–11 km depth in most of the Brawley Seismic Zone (BSZ), and 8–11 km depth beneath the Imperial Fault (Figure 1) [*Lin et al*., 2007; *Hauksson et al*., 2012; *Lin*, 2013]. The entire valley is also characterized by very high heat flow, ~140 mW/m^2 on average [*Lachenbruch et al*., 1985], more than double the average continental heat flow. Volumetrically minor and young volcanism (~2.5 ka) is observed at the Salton Buttes along the

southern shore of the Salton Sea [*Robinson et al*., 1976; *Schmitt and Vazquez*, 2006; *Schmitt and Hulen*, 2008; *Schmitt et al*., 2013].

A huge volume of sediment has been supplied to the Salton Trough and the northern Gulf of California by the Colorado River from erosion of the Colorado Plateau [*Muffler and Doe*, 1968; *Dorsey*, 2010; *Dorsey and Lazear*, 2013]. The Salton Trough is filled with Pliocene and Pleistocene lacustrine and fluvial deposits. This sediment is observed to ~4 km depth in boreholes and is inferred to extend much deeper based on older Pliocene sediments exposed at the basin margins. The sedimentation rate is estimated to be 2–4 mm/yr over the last 0.8 Myr [*Herzig et al*., 1988; *Schmitt and Hulen*, 2008]. Similar rates (1.9–2.3 mm/yr) are suggested for the past 5–6 Myr, which would produce >10 km of sediment [*Dorsey*, 2010].

3. Previous Seismic Work

Numerous studies have used regional seismic networks and local earthquakes to develop three-dimensional (3-D) velocity models in Southern California [e.g., *Magistrale et al*., 1992; *Zhao et al*., 1996; *Hauksson*, 2000; *Magistrale et al*., 2000; *Kohler et al*., 2003; *Lovely et al*., 2006; *Lin et al*., 2007; *Tape et al*., 2009; *Lin et al*., 2010; *Savage and Wang*, 2012; *Lin*, 2013; *Lee et al*., 2014]. *Richards-Dinger and Shearer* [1997] estimated an average crustal thickness of 28 km in Southern California and a Moho depth of 18 km in the Salton Trough by stacking the Moho-reflected phase. *Lekic et al*. [2011], using scattering of teleseismic shear waves, suggested that in the Salton Trough, either the mantle lithosphere has experienced more thinning than the crust or large volumes of new lithosphere have been created. These studies were consistent with a deep sedimentary basin, crust with high seismic velocity, and shallow Moho in the Salton Trough. Some of those models were aided by including information from seismic refraction studies, which provided a much better resolution on the crustal and upper mantle structures due to dense station coverage.

In the Salton Trough, two previous controlled source seismic refraction surveys were acquired to study the basin structure. *Fuis et al*. [1984] and *Kohler and Fuis* [1986] imaged the upper and middle crust throughout the entire Imperial Valley, but neither the Moho-reflected phase *PmP* nor mantle refracted phase *Pn* were recognized to constrain deep crustal structure. The survey of *Parsons and McCarthy* [1996] imaged the Moho at ~21–22 km depth in the Imperial Valley and deepening to ~27 km beneath the Chocolate Mountains east of the valley. However, no *Pn* phase was recorded, and the profile along the axis of the Salton Trough was poorly resolved. *Larkin et al*. [1996] performed low-resolution deep crustal seismic reflection imaging of the transitional crustal structure between the Salton Trough and the Basin and Range province. *Brothers et al*. [2009, 2011] studied basin and fault architecture in the top ~70 m in the Salton Sea using high-resolution chirp seismic reflection data.

In Mexico, multichannel seismic reflection and refraction/wide-angle reflection seismic profiles have been analyzed to image basin structure and rifting styles in the inactive Altar Basin of the southernmost Salton Trough [*Pacheco et al*., 2006; *González-Escobar et al*., 2013], in the northern Gulf of California [*Persaud et al*., 2003; *Gonzalez-Fernandez et al*., 2005; *Aragon-Arreola and Martin-Barajas*, 2007; *González-Escobar et al*., 2009; *Martin-Barajas et al*., 2013], and in the central and southern Gulf of California [*Aragon-Arreola et al*., 2005; *Lizarralde et al*., 2007].

4. SSIP Data

4.1. Data Acquisition

Seven onshore seismic refraction and wide-angle reflection 2-D profiles and two 3-D grids, all recording both inline and offline shots, were acquired by SSIP in 2011 to image the 3-D structure of the Salton Trough (Figure 1) [*Rose et al*., 2013]. Ocean bottom seismometers (OBS) were deployed in the Salton Sea to record both onshore shots and air gun shots in the sea, filling the data coverage gap between the Coachella and Imperial Valleys.

Two types of seismographs were used on land, RefTek 125a "Texans" with single-component 4.5 Hz geophones and RefTek 130's with three-component 4.5 Hz geophones. The sample rate was 4 ms. The OBSs were L-CHEAPO 4 × 4 with four-component system, including 4.5 Hz seismographs and hydrophone. The sample rate was 5 ms. In total, 2762 land seismographs and 50 OBSs were used at 4206 sites, with spacing as dense

Table 1. Shot Information[a]

Shot ID	Size (kg)	Picks Offset Range (km)	Deep Seismic Phases
10000	1440	(−150, 0)	*Pn*, *PmP*
10460	1367	(−130, 50)	*Pn*, *PmP*
10510	229	(−120, 60)	*Pn*, *PmP*
10580	229	(−110, 60)	*Pn*, *Pmp*
10670	458	(−100, 70)	*Pn*, *PmP*
10750	116	(−90, 30)	*PmP*
10770	104	(−90, 80)	*Pn*, *PmP*
10790	69	(−90, 70)	*Pn*, *PmP*
10810	115	(−90, 70)	*PmP*
10830	115	(−90, 80)	*PmP*
10900	115	(−70, 90)	*PmP*
10931	229	(−80, 90)	*PmP*
10932	229	(−70, 70)	*PmP*
10950	115	(−80, 90)	*PmP*
10980	115	(−80, 80)	*PmP*
10990	115	(−70, 80)	*PmP*
11000	115	(−80, 80)	*PmP*
11020	115	(−70, 80)	*PmP*
11030	115	(−70, 90)	*PmP*
11050	120	(−70, 80)	*PmP*
11100	181	(−50, 80)	*PmP*
11620	416	(−80, 130)	*Pn*, *PmP*
11650	115	(−50, 100)	*Pn*, *PmP*
11680	116	(−60, 90)	NA
11800	69	(−60, 90)	*PmP*
11860	115	(−50, 80)	*PmP*
11960	5	(−10, 10)	NA
12000	137	(−10, 10)	NA
12050	229	(−30, 50)	NA
12100	456	(−20, 40)	NA
12220	115	(−20, 120)	NA
12290	456	(−10, 30)	NA
12300	81	(−10, 30)	NA
12330	230	(−3, 5)	NA
12341	1367	(0, 10)	NA
12342	456	(0, 10)	NA

[a]In total, 36 shots were fired along this line. Negative offset is for stations to the north of the shot, while positive is to the south. *Pn* is refraction from the Moho; *PmP* is reflection from the Moho.

as 50 m (Figure 1b). Onshore controlled sources were 126 explosions of 3–1400 kg contained in plugged boreholes, and in the Salton Sea a 3.44 L generator-injector air gun was fired at 2330 locations. Complete details about the survey were described in *Rose et al*. [2013].

This paper is focused on the 250 km long NNW-SSE refraction and wide-angle reflection profile along the axis of the Salton Trough, parallel to the transform faults and relative plate motion direction (Figure 1). The explosive shot information is listed in Table 1. Densely spaced (~3 km) but smaller (~120 kg) shots were fired to provide dense ray coverage of the upper crust in the Brawley Seismic Zone, while larger shots up to 1440 kg were used to produce deep crustal and upper mantle phases (*PmP* and *Pn*). The land seismographs on this profile were all single-component Texans at a spacing of 100 m for smaller explosive shots and 100 or 200 m for larger explosive shots. The receiver spacing in Mexico was 500 m. Thirty-eight OBSs were deployed along the line at ~1500 m spacing. Three hundred sixty-six air gun shots were fired every ~100 m along the line to constrain the upper crustal structure of the Salton Sea. Three gaps in station coverage exist: at the U.S./Mexico border and at the southern shore and the northern shore of the Salton Sea.

4.2. Data Description

Three types of seismic data were recorded: explosive shot-Texan data, explosive shot-OBS data, and air gun shot-OBS data. Air gun shots were also recorded by land seismometers very close to the Salton Sea, but they were not included here due to the short recording offset range and the low data quality. The seismic line went through different environments, including urban areas with vehicle traffic, a shallow water lake, energy plants in a geothermal field, and active farms. The response of onshore seismometers was different from that of the OBSs. Explosive shot size varied, and coupling varied primarily as a result of dry or wet holes. The station spacing was much larger in Mexico and in the Salton Sea. As a result of all these factors, there were systematic variations in noise level and data density along the line.

Representative data sections are shown in Figures 2–6. Data quality is generally best in the farmland of the Imperial and Mexicali Valleys, with the exception of the geothermal field near the Salton Sea. Seafloor OBS data were of good quality, but larger station spacing reduced the ability to correlate low-amplitude phases. Urban noise was high in most of the Coachella Valley, and smaller shots were required due to setbacks from

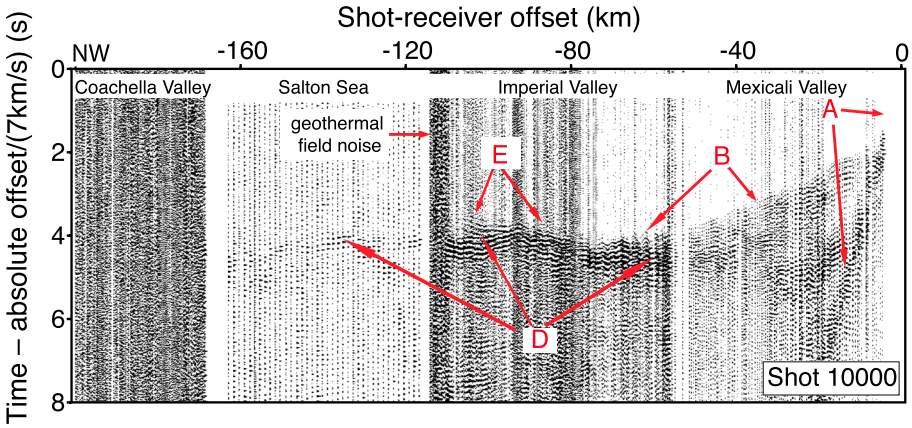

Figure 2. Seismic data for shot 10000. *X* axis is shot-receiver offset with negative value to the northwest, and *y* axis is traveltime reduced by 7 km/s. The data are bandpass filtered by an Ormsby filter 5-8-20-30 Hz. Seismic arrivals are interpreted in the main text. The following phase labels apply for Figures 2–6. A, direct or turning wave in sediment; B, turning waves in the crystalline crust; B′, multiple of B in the sedimentary basin; C, refracted arrival in the Coachella Valley; D, reflection from the Moho; E, refraction from the upper mantle.

structures, such that Coachella Valley data have poorer quality. The air gun was too small to be recorded beyond ~30 km offset but provided excellent control of shallow structure under the Salton Sea [*Kell et al.*, 2012; *Sahakian et al.*, 2016], enabling the explosive shot-OBS data to constrain deeper structure.

At very short shot-receiver offsets, high-amplitude first arrivals "A" with an apparent velocity of ~2 km/s are direct or shallowly refracted waves in the valley sediment (Figures 2–6). These waves continue as very strong

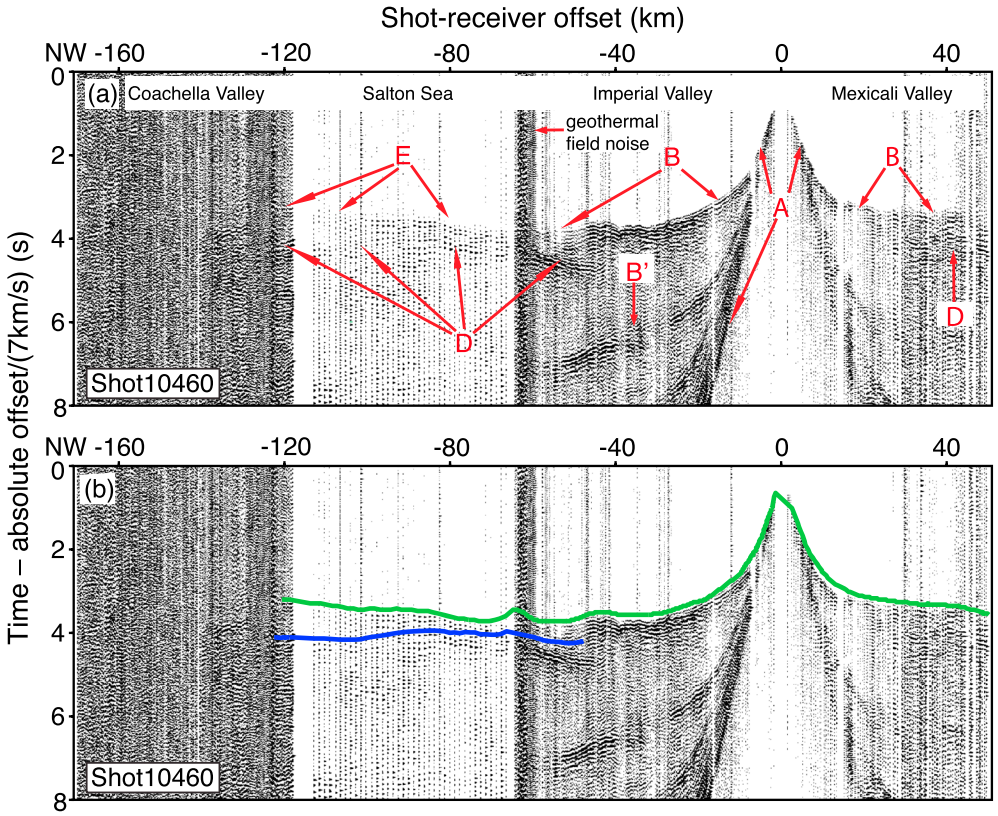

Figure 3. Seismic data for shot 10460, plotted as in Figure 2. (a) Raw data. (b) Data with superimposed arrival times computed from the model of Figure 9. First arrivals are in green, and reflection traveltimes from the Moho are in blue. At some offsets, the green line matches weak first arrivals that are too small to observe in a figure at this scale.

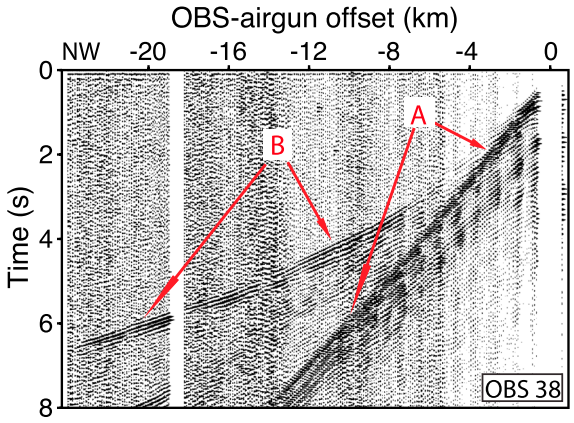

Figure 4. Seismic data for air gun shots recorded on OBS 38, plotted as in Figure 2 but filtered to 5-8-15-18 Hz. The travel-time is not reduced.

secondary arrivals, in part because a strong velocity gradient with depth produces a low-velocity surface waveguide. For all shots that produce shot-receiver raypaths that underlie the Salton Sea, Imperial Valley, and Mexicali Valley, the data are very similar (Figures 2–4 and positive offsets on Figure 5). Shot and OBS gathers in this region are roughly symmetric at positive and negative offsets and observe similar arrivals at similar offsets, indicating an approximately 1-D crustal structure. There are minor variations along the valley, with the strongest being earlier arrivals for shots and stations very close to the Salton Buttes, suggesting thinner sediment at this location. Shots with raypaths that underlie the Coachella Valley have arrivals with different characteristics that will be described below.

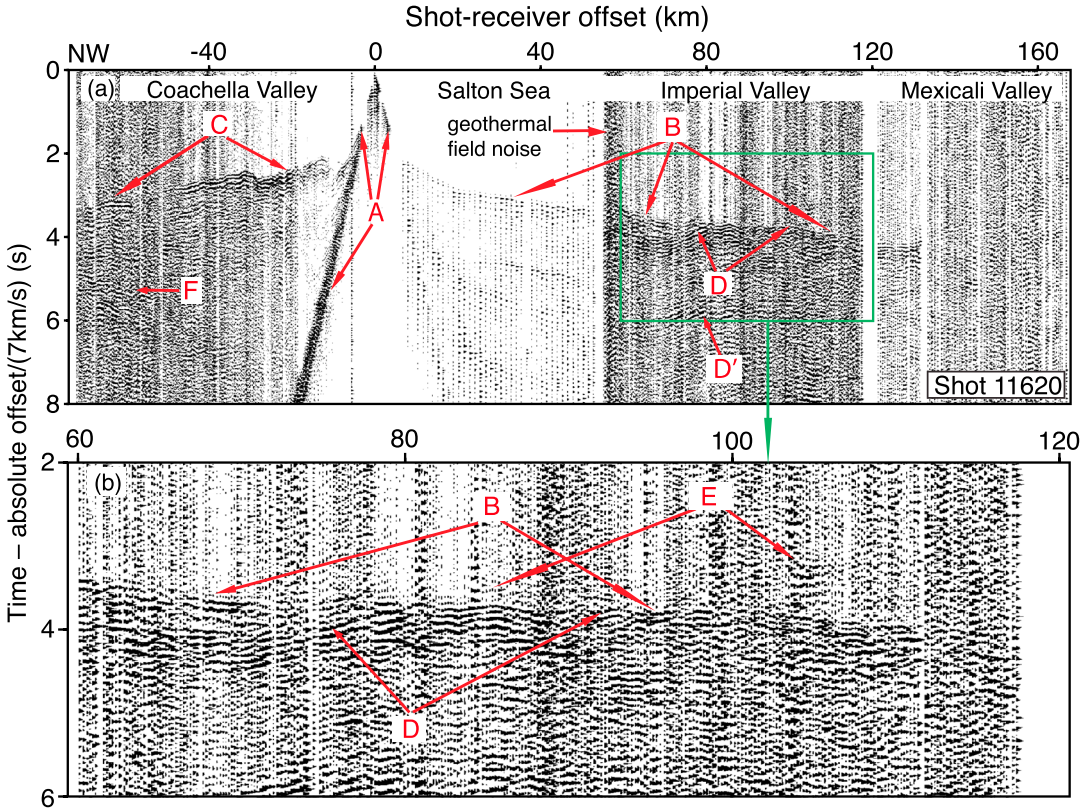

Figure 5. (a) Seismic data for shot 11620, plotted as in Figure 2. Phase D′ is a multiple of D; phase F is reflection from the deeper Moho in the Coachella Valley. (b) Enlarged version of the green box in Figure 5a. *Pn* phase E is weak but can be observed by placing the viewer's eye near the image and looking along the arrival.

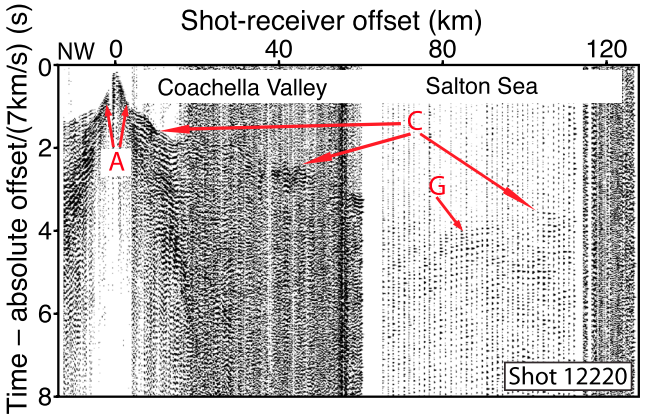

Figure 6. Seismic data for shot 12220, plotted as in Figure 2. Phase G is a possible lower crustal reflection in the Coachella Valley.

A refracted arrival *Pg* phase "B" appears as a first arrival beyond a minimum offset of ~5 km. The transition from arrival A to B is not sharp, and there is no evidence for a reflection corresponding to this refractor. Arrival B has an apparent velocity of ~4 km/s at about 8 km offset but increases to ~5.2 km/s by about 12 km offset and ~6 km/s by about 20 km. The low velocity at near offset is typical of sedimentary rock but quickly becomes greater than 5 km/s, which corresponds to fractured or porous felsic crystalline rock. These changes in apparent velocity are smooth as a function of offset, suggesting that velocity increases smoothly with depth rather than having strong velocity discontinuities in the upper crust. Beyond about 50 km offset, arrival B increases to an apparent velocity greater than 6.6 km/s, corresponding to the lower crust. The long-delay high-amplitude phase B′ is observed and modeled as basin reverberations of phase B by *McMechan and Mooney* [1980] and *Fuis et al*. [1984]. It is caused by the strong vertical velocity gradients in the thick sedimentary basin.

A strong secondary arrival "D" appears at offsets beyond 40 km throughout the Salton Sea and Imperial and Mexicali Valleys (Figures 2, 3, and 5). This arrival has the curvature and strong amplitude typical of a wide-angle reflection from a subhorizontal boundary. The shot-receiver midpoints of this arrival are located from the northern end of the Salton Sea to ~12 km south of the U.S.-Mexico border (*PmP* in Table 1). While this strong arrival is observed at >40 km offset on many shots, only a handful of shots have sufficiently strong signal to record a refracted first-arrival "E" beyond ~80 km offset. E has the correct offset time geometry to be from a refractor corresponding with reflector D (Figures 3 and 5). Arrival E has an apparent velocity of ~7.8 km/s, identifying D and E as the reflection from the Moho (*PmP*) and refraction from the uppermost mantle (*Pn*), respectively. *Pn* is strong on shot 10000 (Figure 2) at the southern end of the line recorded in the northern Imperial Valley and on several shots in the southern Imperial Valley recorded on the OBSs in the Salton Sea (Table 1). Only on one shot can *Pn* be observed on stations in the southern Coachella Valley (Figure 3). Fortunately, shot 11620 in the southernmost Coachella Valley (Figure 5) produced a *Pn* arrival recorded on stations in the Imperial Valley, which, although weak, reverses the *Pn* ray path. The reciprocity of shot-receiver traveltimes with shot 10460 (Figure 2) at the southern end of the Imperial Valley was necessary to identify this arrival in Figure 5; a similar arrival was also observed on shot 11650, which was ~3 km to the north of shot 11620, for a limited offset range of ~10 km. Numerous shots reverse the *PmP* ray coverage beneath the southern Salton Sea and the Imperial Valley (Table 1). At later times than *Pn*, the crustal refraction B with an apparent velocity of ~6.8 km/s and the *PmP* D converge into a single arrival with stronger energy than *Pn* (Figures 2, 3, and 5). A multiple of this phase is also observed as phase D′ on shot 11620 in Figure 5. The very short shot-receiver offsets at which *PmP* (strong beyond 40 km) and *Pn* (first arrival beyond 80 km) are observed indicate a very thin crust; typical continental crust observes those arrivals at almost double those offsets [e.g., *Parsons et al*., 1996].

In the Coachella Valley, the refracted arrival *Pg* phase "C" behaves differently from B (Figure 6 and negative offsets on Figure 5). It has an apparent velocity of ~6 km/s at earlier time from ~10 to >60 km offset, which requires a shallow refractor and a very small velocity gradient beneath. The velocity at the refractor corresponds to unfractured felsic crystalline rock. The sharp changes in arrival time at ~10 km offset to the north of shot 11620 (Figure 5) indicate a near-surface sharp change in basin thickness, which may be fault related or caused by three-dimensional geology and the crooked line geometry. Beneath the Coachella Valley, refracted phase C does not increase to apparent velocity above 6.2 km/s. This is distinctly different from B to the south, which requires the presence of 6.7 km/s at relatively shallow depth. If such a velocity exists under the Coachella Valley, it must be at much greater depth. The apparent velocity and curvature of *Pg* phase B and that of phase C is significantly different, which indicates that the basement in the Coachella Valley is different from that beneath the Salton Sea and the Imperial Valley.

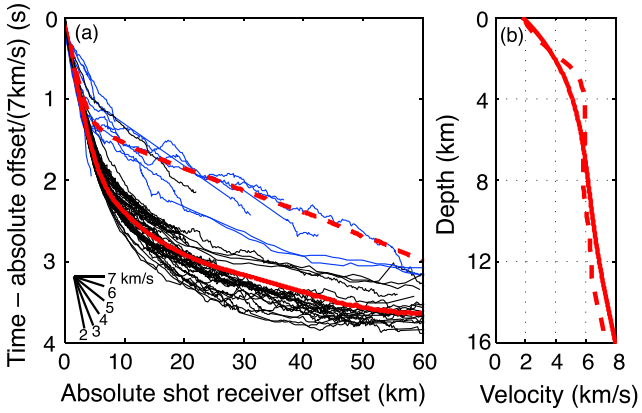

Figure 7. (a) Short-offset first-arrival traveltimes. Black lines correspond to different shots, different directions from each shot, and similar for different OBS receiver gathers. Blue lines correspond to the Coachella Valley. The slopes of different apparent velocities are shown at bottom left. Thick red lines are synthetic first-arrival traveltimes, corresponding to the velocity models in Figure 7b. (b) One-dimensional starting velocity models for the crustal tomography in the Salton Sea, Imperial Valley, and Mexicali Valley (red solid line) and Coachella Valley (red dashed line).

In contrast to the Imperial Valley, most shots do not have long-offset recording and the data quality is too low to constrain the deep crustal structures in the Coachella Valley. Two exceptions are shot 11620 (Figure 5) and shot 12220 (Figure 6). A very weak arrival "F" is observed on shot 11620, and a possible short reflection phase G is recorded on shot 12220. *PmP* phase D in the Imperial Valley is not present on stations in the Coachella Valley for shot 11620. Phase F is tentatively identified as a reflection from a deeper Moho (*PmP*), although no data exist at sufficient offset to identify whether this phase correlates with mantle velocity. The depth corresponding to this reflector is very similar to the regional Moho in Southern California. If phase G is a deep crustal reflection, the arrival time suggests a depth similar to that of the Moho beneath the Salton Sea, but the short recording range limits any further modeling. Because a clearer deeper reflection (phase F) is identified at the same middle point range on shot 11620, phase G is not interpreted as a Moho reflection. Better data are required in order to construct the lower crustal and upper mantle velocity structures in the Coachella Valley, but the observations from SSIP indicate that the middle crust and the Moho in the Coachella Valley are distinct from that beneath the Salton Sea.

5. Analysis Method

Traveltimes of the direct, turning, refracted, and reflected arrivals described above were inverted to produce a seismic velocity model of the crust and uppermost mantle. The three-dimensional (3-D) inversion approach of *Hole* [1992] and *Zelt et al*. [1996] was used. Traveltimes were computed using a finite difference solution of the eikonal equation [*Vidale*, 1990; *Hole and Zelt*, 1995] using a 100 m grid spacing. Times at receivers were interpolated, and rays were found by tracing through the gridded traveltimes. All times and rays were traced in 3-D to include true shot-receiver offsets on the crooked line, but the velocity model was forced to be one-dimensional (1-D) perpendicular to the line. OBSs were receivers for the explosive shots but were also used as shots computing times via reciprocity for the air gun data.

The first arrivals were inverted using traveltime tomography [*Hole*, 1992]. The algorithm used simple backprojection to distribute the traveltime misfit evenly along the whole ray path. The slowness (inverse of velocity) perturbation in a grid cell was calculated from the mean misfit of all the rays traveling through that cell. Where the receivers were unevenly spaced, a weighting parameter was applied to produce a more even weighting by shot gather. A moving average filter was applied to smooth the velocity perturbation before it is added to the previous velocity model. This procedure was iteratively repeated to generate a new 3-D velocity model. The smoothing size of the moving average filter was chosen to be very large in the initial iterations. Smoothing was gradually reduced as the iterations proceed, maintaining a fixed horizontal to vertical aspect ratio. In this manner, misfits were pushed toward large-scale velocity structure, and the starting model for the next iteration was less dependent upon the original starting model. The iteration was stopped when ray smearing began to appear and/or the misfits approximated the picking errors. This approach produced a model with minimal structure required by the data [e.g., *Zelt*, 1999]. Model spatial resolution, which is approximately the final smoothing size, was primarily limited by the shot spacing onshore and OBS spacing in the Salton Sea; these were variable along the line.

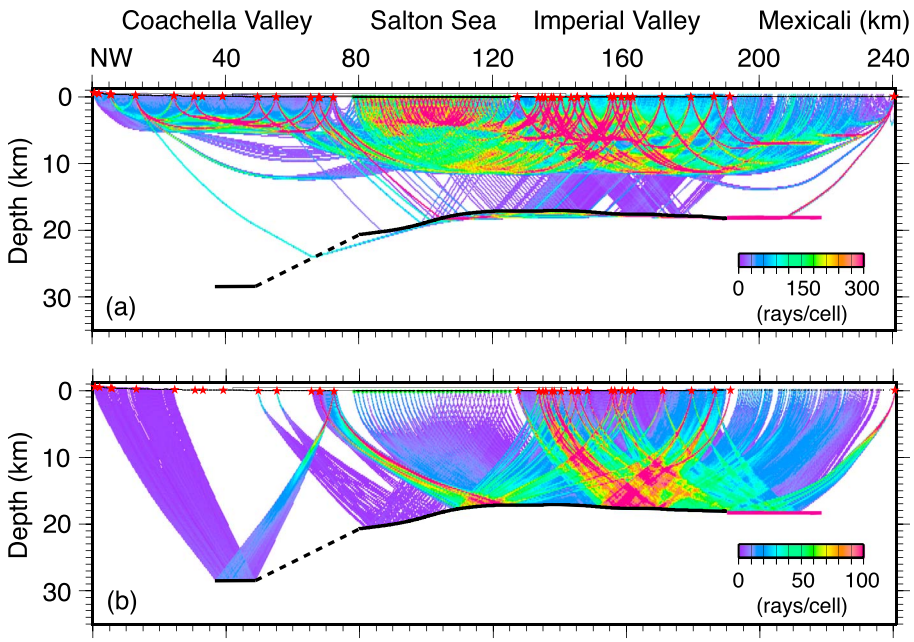

Figure 8. (a) First-arrival ray coverage, including mantle *Pn*, in the velocity model shown in Figure 9. Hit count is for 100 m grid cells. Red stars are the shots, and green circles are the OBSs. (b) Similar ray coverage for Moho reflections *PmP*. The heavy black line in both images is the *PmP* reflector, dashed where not constrained. The thick pink line is a lower crustal reflector in the Mexicali Valley.

The starting velocity model was a very smooth, one-dimensional (1-D) best fit model derived from the first-arrival traveltimes (Figure 7b). Because the data indicated that the Coachella Valley had much thinner sediment and a different crystalline basement, a different starting model was built for the Coachella Valley. Smooth interpolation was applied between the two starting models at the southern end of the Coachella Valley. A horizontal to vertical smoothing ratio of 3:1 was used, which approximated the average orientation of the ray path, more horizontal than vertical.

The first-arrival ray coverage was much denser in the upper crust than in the middle crust (Figure 8). This was due to a decrease in the velocity gradient with depth, constrained by the decreasing curvature of the traveltimes as a function of offset (Figure 7). This also corresponded to a decrease in amplitude and the maximum offset at which the densely spaced smaller explosive shots and the air gun data lost signal. To accommodate this difference in data constraints, and to include deeper arrivals, a layer stripping approach was employed [*Zelt et al*., 1996; *Zelt*, 1999]. This approach determined the shallow velocity structure based on the best data, then fixed the shallower velocity, while modeling deeper structures that had poorer data constraints. The approach was used sequentially for dense first-arrival ray coverage in the uppermost crust, then the sparser first-arrival coverage in the middle to lower crust, next the *PmP* data for the lower crust and Moho, and finally the *Pn* data for the upper mantle.

After the upper crustal velocity model was produced from dense first-arrival traveltimes, the velocity structure above the 6 km/s contour was fixed, and first-arrival tomography was continued. Traveltime misfits for those rays that penetrated this artificial, smooth boundary were applied to the portion of the ray path below the boundary. Due to more horizontal ray paths, sparser large shots that had deeper rays, and larger picking errors due to smaller signal strength, a larger smoothing aspect ratio and a smoother final velocity model with lower spatial resolution was derived for the middle crust (Table 2). The artificial boundary was smoothed in order to remove an artificial discontinuity. This ray coverage extended to a velocity of ~6.7 km/s, but *Pn* with velocity above 7 km/s at offsets greater than ~80 km were not included. The exception was the Coachella Valley, where first arrivals did not reach velocity greater than 6.2 km/s nor penetrate as deep (Figure 8). No first-arrival ray coverage existed in the middle crust under the Coachella Valley at the depths where faster velocity was observed to the south. However, the observed traveltimes were inconsistent with faster velocity, thus directly constraining the middle crust to have a much lower maximum velocity.

Table 2. Model Resolution and Parameters[a]

Model Depth	Smoothing Ratio	Resolution/Smoothing Size (Horizontal/Vertical)	Picking Uncertainty	RMS Misfit
Upper crust	3:1	5 km/1 km	40–50 ms	34 ms
Middle crust	10:1	20 km/2 km	100 ms	85 ms
Lower crust and Moho	20:1	20 km/1 km	220 ms	230 ms
Upper mantle	20:1	100 km/5 km	220 ms	70 ms

[a]Model resolution is represented by the smoothing size in the final iteration of tomography, which is limited by the distance between shots that have reversed ray coverage. The picking uncertainty represents an upper limit, and many picks have better accuracy.

Three-dimensional reflection tomography [*Zelt et al*., 1996] was used to model the wide-angle reflection traveltimes from the Moho (*PmP*). The velocity model was fixed above the 6.7 km/s contour. The Moho interface was horizontally gridded at 200 m spacing. The starting Moho was flat at 18 km. The Moho depth was inverted using a horizontal smoothing of 20 km beneath the Salton Sea and the Imperial Valley and 50 km beneath the Mexicali Valley, depending on the reversed shot interval. This boundary was then fixed, and the remaining misfits were used to invert for seismic velocity in the lowermost crust, keeping the shallower crust fixed. This new lower crustal velocity was fixed to again invert for Moho depth. This procedure was iterated until the root-mean-square (RMS) misfit stopped decreasing. In this study, the minimum misfit was reached using a laterally near-homogenous lower crust.

The crustal velocity model and the Moho depth were then fixed, and *Pn* was used to model the upper mantle velocity. The upper mantle velocity was kept very smooth (Table 2) because the data reversal distance was ~120 km. The data coverage is only sufficient to detect a large-scale lateral change in mantle velocity. The data only constrain the uppermost mantle lid and not deeper mantle velocity structure.

First arrivals and secondary refractions and reflections were picked manually on all the shot gathers (Table 1). The full period of the dominant signals increases from ~80 ms at near offset (<20 km) to ~110 ms at far offset (>50 km). The estimated accuracy of the upper crustal first arrivals is less than a half period, which is 40–50 ms (Table 2). The uncertainty of first arrivals used in the middle crustal tomography is within one full period due to weaker signal at further offset. Dense onshore recording helped improve the picking accuracy, while sparser OBSs increased the uncertainty for weak arrivals. The uncertainty of Moho reflection (*PmP*) and mantle refraction (*Pn*) picks is within one full period for a high-quality recording (e.g., phase E in Figure 2 and phase D at −50 km offset in Figure 3), but many picks are within two full periods (e.g., phase D in the Salton Sea in Figure 3 and phase E in Figure 5). The picking uncertainty represents an upper limit (Table 2), and many picks have better accuracy. In addition, it is more likely to pick a late cycle than a time that precedes the actual arrival.

6. Seismic Velocity Model

The seismic velocity model of the entire crust and uppermost mantle (Figure 9) was generated from all of the arrivals discussed in section 4, using the method described above. Figure 8 shows ray coverage, and Figures 10 and 11 and Table 2 show data misfits.

6.1. Upper Crust

Very dense shot, receiver, OBS, and air gun spacing provide excellent ray coverage of the upper crust, to a depth of ~7–8 km (Figure 8), corresponding roughly to the 6 km/s contour (Figure 9). The shallowest velocity is ~1.8 km/s, representative of unconsolidated, water-saturated valley sediment, but increases rapidly as a function of depth. Details in the sediment are smoothed by the tomography. However, phase B in the seismic data (Figures 2–5) includes first arrivals with apparent velocities that increase rapidly and smoothly with distance from ~4 to >6 km/s (Figure 7). This provides evidence for a strong, smooth velocity gradient with depth, with no evidence for discontinuities. Velocity increases from values typical of unconsolidated sediment to values faster than clastic sedimentary rock (<5 km/s) [*Christensen and Mooney*, 1995], requiring crystalline rock within the bottom part of this gradient zone. Beyond ~4 km/s, the apparent velocity changes more slowly as a function of offset, indicating a decreasing velocity gradient with depth. The 4.0 km/s and overlying contours are relatively flat from the northern Salton Sea to the northern Mexicali Valley, with

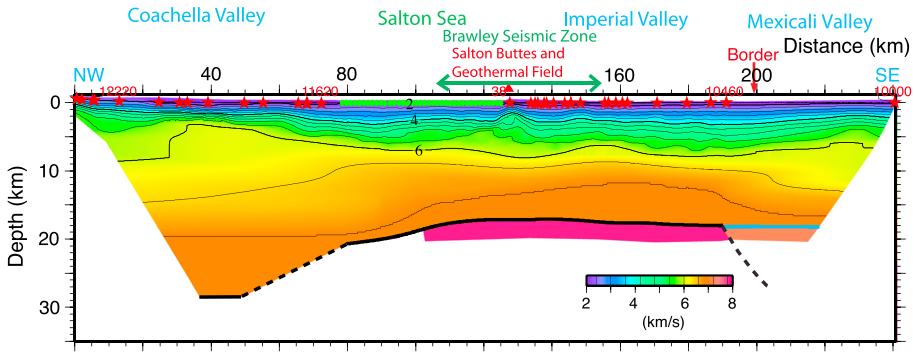

Figure 9. Seismic velocity model along the axis of Salton Trough. Red stars are explosive shots, and green circles are OBSs. Contour interval is 0.4 km/s. The thick black line below 6 km/s is the strong Moho reflector, dashed where not directly constrained. The thick cyan line is a lower crustal reflector in the Mexicali Valley. Regions without ray coverage are white. Numbered shots and OBS are shown in data Figures 2–6.

4.0 km/s at ~3 km depth. A notable exception is a ~10 km wide zone beneath the Salton Buttes, where velocity contours $<$5.0 km/s are ~1.5 km shallower.

However, shallow velocity structure in the Coachella Valley is distinctly different. Sediment thins to the north and contains local, likely fault-bounded basins. These basins are illustrated by rapid lateral changes in traveltime that correlate with receiver position (e.g., at offset of 10 and 30 km to the north in Figure 5); these small subbasins are not well represented by the velocity model due to the urban noise in the data and the larger smoothing used in the Coachella Valley tomography. The shot gathers show a much sharper increase in apparent velocity from ~2 km/s to ~6 km/s, and velocity near 6 km/s persists to long offsets (Figure 7). Basement has a seismic velocity of 6–6.2 km/s typical of felsic (granitic) crystalline rock. The basement boundary is vertically smoothed by the tomography. A thicker basin and slower basement velocity are indicated at the northern end of the line, where the line obliquely crosses multiple strands of the San Andreas Fault system (Figure 9).

The southern end of the line is constrained by a shot in the southwestern corner of Arizona that is reversed by several shots in the southern Imperial Valley, but there were no shots for 50 km in Mexico (Figure 1). Although not as well constrained, velocity contours representing sediment are shallower toward the south end of the

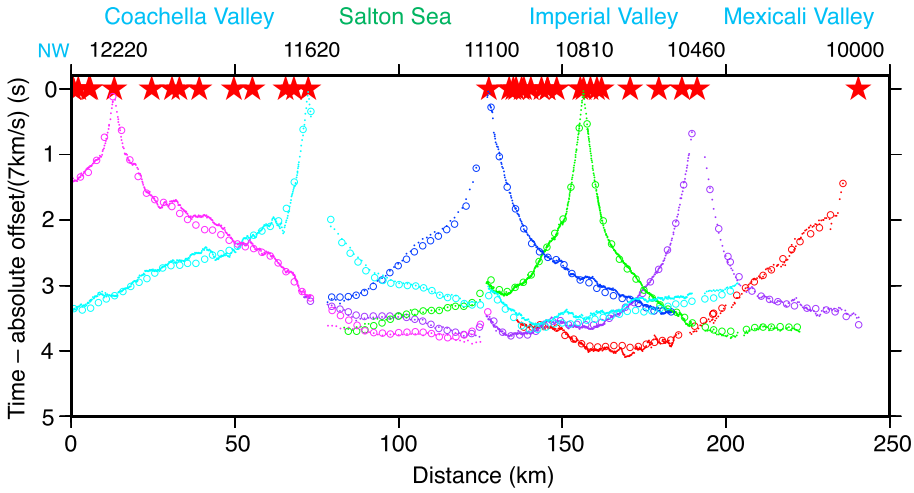

Figure 10. First-arrival, including *Pn*, picks and synthetic traveltimes of six shot examples, are shown with a reduced traveltime of 7 km/s. Picks are plotted at the location of the receiver. Red stars are shots, with example shots numbered. Dots in different colors are picks, and circles are corresponding synthetic traveltimes for different shots. Synthetic traveltimes only every 3 km are plotted for clarity. Circle size is 100 ms.

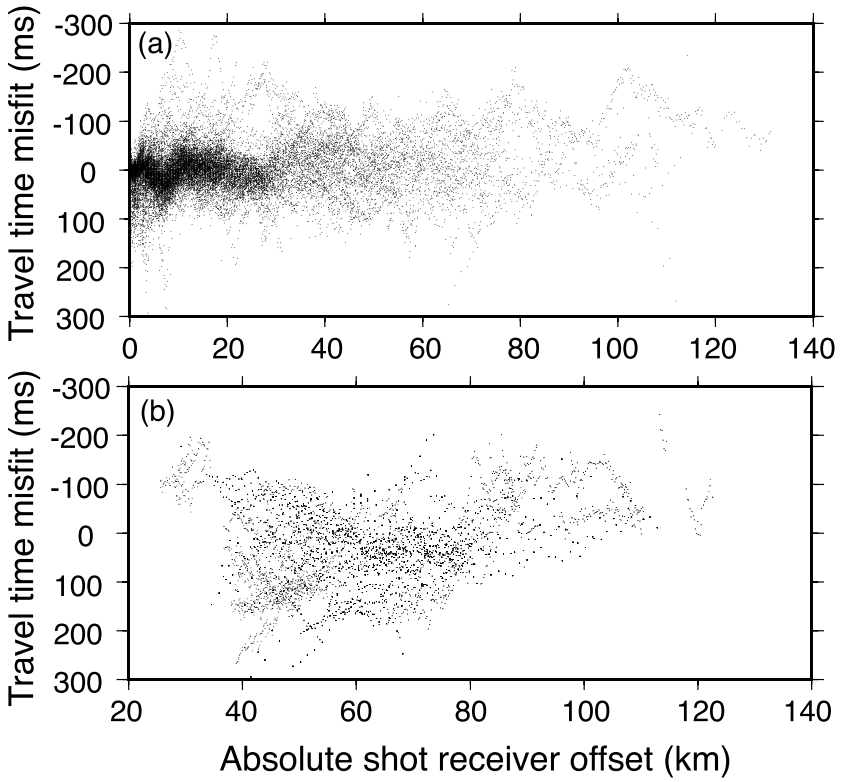

Figure 11. Misfit (calculated minus observed) versus absolute shot-receiver offset for (a) first arrivals, including *Pn* and (b) *PmP*.

line, while underlying contours are deeper (Figure 9). This may be due to the Arizona shot being somewhat offline, closer to the edge of the Salton Trough.

6.2. Middle Crust

Below 7–8 km depth, or ~6 km/s, in the Salton Sea and the Imperial Valley, the velocity gradient with depth continues to decrease. This means that first arrivals from these depths arrive at much longer offsets and with lower amplitudes. They are not recorded from the air gun shots and only partly recorded from the small explosive shots due to low signal-to-noise ratio on the OBS records. As a result, the spatial resolution in the middle crust is not as good, and a larger lateral smoothing was used in the tomography (Table 2). However, the larger shots indicate that apparent velocity continues to increase with offset (except in the Coachella Valley) but at a slower rate. Beyond ~90 km, the first-arrival phase B becomes a secondary arrival behind the upper mantle refraction (e.g., Figures 2 and 5 as a long-offset secondary arrival). The maximum apparent velocity of this phase is ~6.8 km/s. This continuous increase in apparent velocity with offset indicates a sufficient velocity increase with depth that first-arrival turning rays provide continuous, overlapping ray coverage down to ~12 km depth (Figure 8), where the velocity is 6.7–6.8 km/s (Figure 9). While the velocity gradient from 7 to 12 km depth is much smaller than in the upper crust, it is a relatively large gradient for normal continental crust [*Christensen and Mooney*, 1995]. The persistence of the 6.8 km/s refracted phase to long offsets without a further increase in velocity indicates that velocity does not continue to increase below ~12 km depth. The change in velocities from $<$6.5 km/s to $>$6.7 km/s requires a change in lithology [*Christensen and Mooney*, 1995], but no reflector is observed. We will thus interpret this change in velocity gradient and change in lithology as a compositional boundary that is gradational over ~1 km depth. The depth of this boundary is accurate to ~1 km.

Basement below the 6 km/s contour in the Coachella Valley is very different from that to the south (Figure 9). It is characterized by a much smaller velocity gradient, which is directly constrained by the data that do not observe an apparent velocity $>$6.2 km/s. Although the internal structure of the middle crust is not

constrained by sufficient turning ray coverage (Figure 8), its velocity must be much slower than that beneath the Salton Sea and the Imperial Valley or higher velocity would be observed as first arrivals in the data. The data do not allow velocity >6.5 km/s shallower than ~13 km depth nor velocity >6.8 km/s shallower than ~18 km depth.

The Mexicali Valley is not as strongly different from the Imperial Valley, but also has slower velocity at 9–14 km depth (Figure 9). This is in contrast to the shallow velocity, which is a little faster than to the north. The location of this lateral change is not well constrained due to the lack of shots in Mexico, but it is not far south of the U.S.-Mexico border.

6.3. Lower Crust and Moho

Beneath the Salton Sea and the Imperial Valley, strong first and secondary turning wave arrivals (phase B in Figure 5) directly constrain a velocity of 6.7–6.8 km/s at ~12 km depth (discussed above, Figure 9). Deeper crustal velocity is constrained by dense, reversed *PmP* ray coverage (Figure 8b). As a secondary arrival, *PmP* has larger picking errors (Table 2) and may be consistently picked one or more cycles (~110 ms per cycle) early or late. The estimated picking error and RMS misfit (Table 2) allow ~1 km of uncertainty in Moho depth and a lower crustal velocity of 6.7–6.8 km/s. This independently derived velocity is consistent with the refracted arrivals from the top of the layer and with the absence of a 6.9–7.5 km/s refracted arrival. The Moho is relatively flat at 17–18 km depth (Figure 9). Beneath the northern Salton Sea, the Moho is 2–3 km deeper and dips to the north, constrained by strong but unreversed reflections recorded by OBSs from shots in the southern Coachella Valley. The Moho is shallowest (~17 km depth) beneath the Brawley Seismic Zone, but the difference of <1 km is within the uncertainty range of the model.

The strong *PmP* reflection at 45–90 km shot-receiver offsets, observed in all of the data underlying the Imperial Valley and Salton Sea (phase D in Figures 2, 3, and 5), is absent in data beneath the Coachella Valley. In the Coachella Valley, deep crustal phases are only observed from two shots with poor data quality, which results in large uncertainties for the middle and lower crustal structure in this area. The first is in shot gather 11620, which observes an unreversed reflection phase F (Figure 6), which suggests a reflector at ~28 km depth. The other is shot gather 12220, in which reflection phase G looks similar to *PmP* to the south but is at much larger shot-receiver offset and only recorded for ~10 km offset range. The reflector G is roughly at 18–19 km depth and distance of 50–60 km, but no *Pn* is recognized. We interpret this reflector as the boundary between the middle and lower crust, and the ~28 km deep reflector as Moho, primarily because it is almost as deep as Moho observed in surrounding areas [*Richards-Dinger and Shearer*, 1997].

6.4. Upper Mantle

Pn phases are recorded by six shots across an offset range of >20 km, well establishing the apparent velocity, and by three additional shots with only a short segment (Table 1). The low signal strength of *Pn*, especially on shot 11620 (Figure 6), produces a larger picking error. Picking errors are likely correlated within each shot gather, and are non-Gaussian due to the possibility of cycle skips. Picking a late cycle is more likely than an early pick. However, the slope of the picks is much better constrained than precise time, and the slope is the primary constraint on mantle velocity. A uniform upper mantle with a velocity of 7.85 km/s provides an excellent fit to all the *Pn* phases except shot 10000. The modeled *Pn* traveltimes are systematically later than the picks by almost 100 ms for shot 11620. This may be because the middle and lower crust (beneath 10 km depth), through which the shot 11620 *Pn* travels, is poorly constrained due to very limited ray coverage (see Figure 8).

The apparent velocity of the *Pn* arrival on shot 10000 is consistent with the same upper mantle velocity, but the observed *Pn* arrival times are about 250 ms later than the synthetic arrival time, much larger than the estimated picking error for this shot (~110 ms, Figure 2). Unfortunately, this phase is not reversed; no shot recorded *Pn* on the more sparsely spaced receivers in Mexico. The reflections observed under the Mexicali Valley constrain the depth of the reflector (thick cyan line in Figure 9), which is very similar to the Moho under the Imperial Valley. Yet, the *Pn* phase from shot 10000 arrives much too late for this reflector to be Moho. Because *Pn* and the reflection have similar ray paths above the reflector, the *Pn* traveltime above the reflector is well constrained. Therefore, the *Pn* delay must occur below the reflector. For this reason, a velocity of 7.2 km/s was required beneath the Mexicali reflector, indicating it is not Moho. The location of the change from 7.85 to 7.2 km/s (km 190 in Figure 9) is poorly constrained. However, moving it farther north by

~10 km requires faster velocity (~7.5 km/s) below the Mexicali reflector, and moving it farther south cannot effectively delay the *Pn* from shot 10000, because the *Pn* ray will travel directly to the mantle rather than along the reflector. In addition, to make the synthetic *Pn* traveltimes consistent with observations, velocities greater than 7.8 km/s must occur at least 5 km deeper than this reflector, as indicated by the dashed line at the south end of Figure 9.

7. Comparison With Previous Refraction Models

The seismic data and the velocity model in this paper are consistent with the upper crustal model down to 6–8 km depth within the Imperial Valley by *Fuis et al*. [1984] and *Kohler and Fuis* [1986]. This includes the high velocity gradient in the upper crust, basin thickness of 3–5 km, and much thinner basin localized near the Salton Buttes. With many more shots and stations, SSIP provides better spatial resolution. However, the middle and lower crust of *Fuis et al*. [1984] is not similar to Figure 9, as they regionally include a "subbasement" refractor with velocity >7 km/s dipping north along the valley at 10–16 km depth. East of the Imperial Fault, the seismic data of the two projects contain similar arrivals, but they are interpreted differently here due to SSIP's much denser station spacing that allows excellent correlation of phases. Our shot 10460 (Figure 3) was intentionally colocated with shot point 6 of *Fuis et al*. [1984], and the reversed line between their shots 6 and 13 is subparallel to our line. The dipping 7 km/s refraction from their shot 6 on their line (Figure 8 of *Fuis et al*. [1984], which has a different reducing velocity) is consistent with the upper crustal refraction phase B in SSIP Figure 3, but their reversed refraction arrival from their shot 13 is the *PmP* phase described in this paper. This reinterpretation of their arrivals using SSIP's denser data replaces their >7 km/s dipping subbasement with structure similar to Figure 9.

Parsons and McCarthy [1996] analyzed data from a densely sampled profile that started in the southern Imperial Valley and headed northeast into Arizona and a second much sparser profile that ran along the western Imperial Valley and the western margin of the Salton Sea and Coachella Valley. The first line densely sampled the middle and lower crust only at the eastern margin of the valley and mountains to the east. Their line along the axis of the Salton Trough had only five shots and is described as being poorly constrained. Two reflectors at ~16 and ~22 km were reported along the Salton Trough line, and the deeper one was identified as Moho. Given the large uncertainty in their middle and lower crustal velocity, and the location of the northern two thirds of their line at the valley margin, SSIP's results are better constrained and probably more representative of the central axis of the valley.

8. Salton Trough Rift Structure and Processes

8.1. Crustal Structure in the Salton Trough

Thick sediment with low seismic velocity (<2 to ~4 km/s) from the Colorado River was deposited in the Salton Trough at a rate of 2–4 km/Myr. The minimum sediment thickness as constrained by seismic velocities is ~3 km beneath the Salton Sea, the Imperial Valley, and the Mexicali Valley and only ~1.5 km in the Salton Sea geothermal field. Low velocity gradually shallows toward the northern Coachella Valley. The seismic velocity above and beneath this depth continuously increases with depth due to compaction, cementation, and hydrothermal and metamorphic alteration.

Under the Salton Sea and the Imperial Valley, the seismic velocity increases to ~5 km/s at ~4 km depth, which is too high for sedimentary rocks and is likely felsic crystalline rocks. The seismic velocity is still much lower than unfractured granitic rocks [*Christensen and Mooney*, 1995] or than basement in surrounding mountains [*Parsons and McCarthy*, 1996]. One interpretation is that seismic velocity could be reduced by fracturing, but it is slow throughout the entire valley, not just in the active BSZ. The effects of fractures are likely partially compensated by hydrothermal alteration. No reflection is observed at the top of the crystalline rocks, which suggests a transitional boundary rather than depositional discontinuity between sediment and crystalline rocks. These crystalline rocks were previously interpreted as young Colorado River sediment metamorphosed by high heat flow in the Imperial Valley [*Fuis et al*., 1984]. SSIP constrains the velocity increase with depth with more details than the 1979 data set but is consistent with and reinforces this interpretation (Figure 12). Marine reflection imaging in the Salton Sea observes stratigraphic boundaries in the crystalline rocks below 4 km depth, placing greater confidence that the velocity structure represents a gradational metamorphic transition.

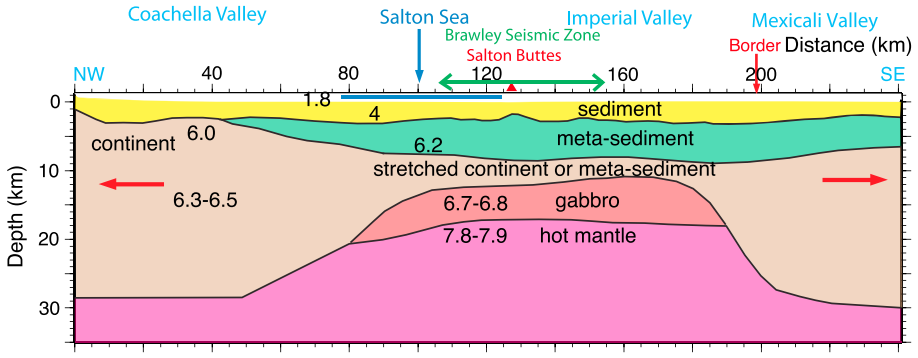

Figure 12. Geological interpretation of rift structure derived from the velocity model. Values in each layer are compressional wave velocities in km/s.

Under the Salton Sea and the Imperial Valley, the seismic velocity continues to increase in the middle crust and reaches a lower crustal velocity of 6.7–6.8 km/s. The velocity of 6.2–6.6 km/s in the middle crust is consistent with the felsic-intermediate composition middle and lower continental crust of Southern California. Alternatively, this velocity could result from continued metamorphism of older, deeper Colorado River sediment to higher amphibolite or granulite grade. This ~4.5 km thick layer could be either stretched preexisting continental crust or young metasedimentary rock, possibly including minor basaltic intrusion (Figure 12).

The lower crust has a layer 5–6 km thick with a seismic velocity of 6.7–6.8 km/s (Figure 9), constrained by a 6.8 km/s refracted arrival and independently by curvature of the *PmP* traveltimes. A velocity >6.7 km/s is consistent with gabbroic rock at the high temperatures expected at depth in the rift [*Christensen and Mooney*, 1995] and is not observed elsewhere in Southern California crust. This layer is interpreted to be underplated mafic magmatic material associated with partial melting of the upwelling asthenosphere in the rift (Figure 12). Basaltic xenoliths with mid-ocean ridge chemistry are found in the Salton Buttes [*Schmitt and Vazquez*, 2006], supporting this interpretation. The upper mantle lid velocity of 7.85 km/s is ~3% lower than the global average [*Christensen and Mooney*, 1995], indicating high temperature. Teleseismic body wave tomography indicates that the upper mantle seismic velocity is at least 2% slower than the regional mean from 60 to 160 km depth beneath the Salton Trough [*Schmandt and Humphreys*, 2010]. The 7.85 km/s velocity requires a mantle temperature near the ~1060 °C basalt solidus at 18 km depth [*Perry et al.*, 2006].

A very different crystalline rock velocity structure is observed beneath the sedimentary basin of the Coachella Valley. A sharper boundary is indicated by a sharper transition from ~2 km/s phase A to ~6 km/s phase C in the seismic data and very low velocity gradient with depth in the basement (Figure 9). This velocity and gradient are typical of intact felsic crystalline rock [*Christensen and Mooney*, 1995]. While ray coverage is not dense in the middle crust under the Coachella Valley (Figure 8), the first-arrival data constrain the velocity from ~7 to ~16 km depth to be much slower than that beneath the Salton Sea. If Salton Sea seismic velocity structure existed at the same depths beneath the Coachella Valley, it would create a faster first arrival that is inconsistent with the data (Figure 5 and 6). For these reasons, despite the lack of turning ray coverage, the velocity model must have much slower velocity under the Coachella Valley than under the Salton Sea (Figure 9).

Similarly, the strong *PmP* reflection observed at 40–80 km offset under the Salton Sea and the Imperial Valley is absent beneath the Coachella Valley. The deeper seismic reflector F observed in Figure 5 at ~28 km depth (Figure 9) is interpreted to be Moho. No *Pn* arrival is observed to confirm this interpretation, but 28 km is almost as deep as the Moho beneath the surrounding ranges [*Parsons and McCarthy*, 1996; *Richards-Dinger and Shearer*, 1997]. Based on these observations, the Coachella Valley sedimentary basin is interpreted to be deposited on modestly extended preexisting granitic continental crust of the Peninsular Ranges (Figure 12). The transition from weakly extended preexisting crust with a deep Moho to strongly attenuated or broken crust with a very shallow Moho occurs beneath the southernmost Coachella Valley.

Structure beneath the Mexicali Valley is constrained by reversed data but at a much larger shot and receiver spacing (Figure 8). Sedimentary basin structure appears similar to the Imperial Valley but is only ~3 km thick (Figure 9), consistent with a well near the southernmost shot point [*Pacheco et al.*, 2006]. The velocity of the

shallowest crystalline rocks increases rapidly to ~6 km/s, then there is a much lower gradient than beneath the Imperial Valley (Figure 9). This basement structure is more similar to the Coachella Valley. At 9–14 km depth, the velocity is much lower beneath the Mexicali Valley than the Imperial Valley (Figure 9). While a strong reflector is observed that resembles the *PmP* beneath the Imperial Valley, seismic velocity beneath this reflector must be 7.2–7.5 km/s (Figure 9). The nature of this reflector is unclear, and it is awkward that the depth is so similar to the Moho to the north; however, a clear *Pn* phase on the southernmost shot 10000 (Figure 2) requires that Moho be at least 5 km deeper than this reflector beneath the Mexicali Valley (Figure 9). Better data coverage across the U.S.-Mexico border is needed to better understand the transition in crustal structure beneath the border. Due to the bend in the seismic line, this crustal structure may represent the transition toward the eastern edge of the Salton Trough rather than the entire Mexicali Valley.

We interpret the shallower sedimentary basin in the upper crust, lower velocity in the middle crust, and deeper Moho beneath the northern Mexicali Valley as stretched continental crust (Figure 12). It may be thinner than beneath the Coachella Valley, and the lowermost crust has a high velocity that suggests rift-related mafic intrusion. Inline with the SSIP line to the south-southeast is the Altar basin in northern Sonora (Figure 1c) [*Pacheco et al*., 2006]. In the central and northern Gulf of California, a series of rift basins, including the Altar basin, along the eastern side of the Gulf became inactive when rifting jumped northwestward to the currently active rift centers ~3 Myr ago [*Stock*, 2000; *Aragon-Arreola and Martin-Barajas*, 2007]. Between these inactive rifts and the active rifts is a thicker block of thinned continental crust [e.g., *Martin-Barajas et al*., 2013]. We interpret the seismic velocity structure and thicker crust beneath the Mexicali Valley as a similar block of stretched continental crust between the older, inactive Altar Basin and active Imperial Valley-Salton Sea rift (Figure 12). The boundary between this block and the Imperial Valley crust lies close to the Mexico-U.S. border.

8.2. Rifting Processes in the Salton Trough

The crust and upper mantle model in Figure 12, which is parallel to the relative plate motion direction, illustrates a strongly extended rift zone with 17–18 km thick crust that is ~100 km wide. The remarkably 1-D structure and flat Moho suggest that active extension in the lower crust and upper mantle is widely distributed and ductile across this ~100 km width. Because neither localized Moho topography nor mantle velocity anomalies are observed, and the middle crust seems not to be affected by locally focused magmatism, we interpret that there is no localized seafloor spreading center beneath the thick sediment of the Salton Trough. Instead, the lower crust is formed by mafic intrusion by distributed underplating from partial melting of the hot upper mantle. Based on thermal arguments, *Lachenbruch et al*. [1985] came to a similar conclusion that magmatism must be broadly distributed. The preexisting continental crust has either totally ruptured or been ductilely stretched to at most 5 km thick (Figure 12). This layer must be hot and ductile in the rift's high heat flow. The broadly distributed magmatism and ductile extension in the lower crust contrasts with relatively localized brittle deformation in the Brawley Seismic Zone and very localized volcanism at the Salton Buttes.

Using a constant rifting rate of ~2 cm/yr, which is the current motion on the southern San Andreas Fault, the 100 km wide rift means that the continent started to break apart ~5 Myr ago. The San Andreas Fault and Salton Trough rifting rates may have been faster prior to initiation of the San Jacinto Fault ~1.2 Ma [*Kirby et al*., 2007]. If rifting jumped from the Altar Basin to the Imperial Valley ~3 Ma [*Aragon-Arreola and Martin-Barajas*, 2007], then continental stretching or breakup had to occur more quickly. This rifting exploited older extension in the southern Basin and Range [*Stock*, 2000], including a low-angle detachment in the Salton Trough region [*Axen and Fletcher*, 1998]. Most or all (at least 13 km) of the existing 17–18 km thick crust formed by sedimentation from above and magmatism from below (Figure 12). Felsic crystalline rocks of this crust include metamorphosed sediment and perhaps pieces of highly stretched continent. Along passive continental margins, mostly new crust formed by these processes could easily be misinterpreted as stretched preexisting continental crust.

8.3. Comparison Along the Gulf of California: The Role of Sedimentation During Rifting

The cross section of Figure 12 can be compared to similar cross sections parallel to the relative plate motion direction across other rift segments of the Gulf of California [*Gonzalez-Fernandez et al*., 2005; *Lizarralde et al*., 2007; *Martin-Barajas et al*., 2013]. These sections show a transition from sediment-free in the southern Gulf to

sediment-filled in the northern Gulf and Salton Trough. In the southern and central Gulf, the continent has ruptured and seafloor spreading has created hundreds of kilometers of oceanic crust. In some of these rift segments, the continent broke after little extension in the plate motion direction, creating a sharp boundary between thick continental crust and oceanic crust, while other segments stretched the continent hundreds of kilometers before rupture [*Lizarralde et al*., 2007]. Sediment thickness on these mid-ocean ridge segments is 0 km in the southern Gulf to 2–4 km in the central Gulf.

The northern Gulf of California has a sedimentation rate almost as high as the Salton Trough. The northern Gulf contains the active Delfin basins in the northwest and the inactive Tiburon Basin in the southeast (Figure 1a), similar to the relationship between active Salton and the inactive Altar basins. The Tiburon Basin and an intrabasin structural high are both underlain by strongly extended continental crust [*Gonzalez-Fernandez et al*., 2005; *Martin-Barajas et al*., 2013]. In the Delfin Basins, the continent is interpreted to have ruptured relatively recently, creating 25–40 km of new crust by magmatism and sedimentation [*Martin-Barajas et al*., 2013]. Stretched continental crust beneath the Mexicali Valley (Figure 12), between the active Salton and inactive Altar basins, is interpreted to be similar to the intrabasin high between the active Delfin and inactive Tiburon basins. However, the larger Salton basin is interpreted to have broken or substantially stretched the continent 2–4 Myr ago, creating ~100 km of new crust with steep margins to thicker crust. In comparison, the continent stretched more and broke later in the Delfin Basin. These differences are similar to those observed by *Lizarralde et al*. [2007] in adjacent rift segments in the southern Gulf of California.

In both the Delfin and Salton Trough basins, the preexisting crust has essentially rifted apart, but seafloor spreading has not initiated. This is because sedimentation, metamorphism, and magmatism create new crust to compensate crustal thinning and to maintain the crustal thickness. Both the maximum earthquake depth of $\leq$11 km in the Brawley Seismic Zone [*Hauksson et al*., 2012] and the approximately 1-D rift structure of Figures 9 and 12 indicate that the lower crust is ductile throughout the Salton Trough, consistent with the very high heat flow. The combination of ductile flow in the lower crust and widely distributed sedimentation and metamorphism in the upper crust heal incipient weakening or thinning. Strain localization would require either a thinner curst or a greater extensional force. Although thick sedimentation promotes rift localization in the early stage of rift evolution due to buoyancy effects [*Bialas and Buck*, 2009], it delays crustal breakup and the initiation of seafloor spreading in the late stage.

9. Conclusions

The SSIP data constrain the crust to be 17–18 km thick and roughly one-dimensional from the northern Salton Sea to the southern end of the Imperial Valley. In the central Salton Trough, crystalline rocks ($>$5 km/s) occur at ~4 km depth and are interpreted to be sediment metamorphosed by high heat flow to ~8 km depth. Crystalline rocks with velocity of ~6.2–6.6 km/s are ~4.5 km thick and are interpreted to be either stretched preexisting continental crust or high-grade metamorphosed sediment, with possible minor basaltic intrusion. A high velocity of 6.7–6.8 km/s in the lower crust is interpreted as rift-related mafic intrusion by underplating. The upper mantle velocity is 7.85 km/s, indicative of high heat and partial melting. In contrast, in the Coachella Valley, sediment thins to the north, the crust thickens, and the basement is interpreted to be granitic continental crust. The Mexicali Valley is also interpreted to be underlain by thicker stretched continental crust. North American crust has been essentially rifted apart with steep continental margins. Since breakup, an ~100 km wide zone of new crust in the extensional direction has been created by magmatism from below, sedimentation from above, and metamorphism of the sediment. The active rift zone is interpreted to be at least ~100 km wide in the lower crust and upper mantle, despite the much narrower volcanic, thermal, and seismic features in the uppermost crust. The Salton Trough and northern Gulf of California emphasize the important role of river delta sedimentation upon late-stage rifting.

Acknowledgments

This research was supported by NSF MARGINS and EarthScope grants 0742263 to J.A.H. and 0742253 to J.M.S., by NSF Marine Geology and Geophysics grant 0927446 to N.W.D. and G.M.K., by the U. S. Geological Survey's Multihazards Research Program, and by the Southern California Earthquake Center (SCEC) (contribution 6244). SCEC is funded by NSF cooperative agreement EAR-1033462 and USGS cooperative agreement G12AC20038. We thank the $>$90 field volunteers and USGS personnel who made data acquisition possible. Numerous landowners allowed access for shots and stations and are acknowledged in *Rose et al.* [2013]. Seismographs and technical support were provided by the IRIS-PASSCAL instrument facility; special thanks go to Mouse Reusch and Patrick Bastien from PASSCAL for their field and data efforts. We also thank the Associate Editor and two anonymous reviewers for their helpful and constructive reviews. The data have been archived at the IRIS DMC (ds.iris.edu/pic-ph5/metadata/SSIP/form.php).

References

Aragon-Arreola, M., and A. Martin-Barajas (2007), Westward migration of extension in the northern Gulf of California, Mexico, *Geology*, *35*, 571–574, doi:10.1130/G23360A.1.

Aragon-Arreola, M. J., M. T. Morandi-Soana, J. A. Martin-Barajas, L. A. Delgado-Argote, and A. Gonzalez-Fernandez (2005), Structure of the rift basins in the central Gulf of California: Kinematic implications for oblique rifting, *Tectonophysics*, *409*, 19–38.

Axen, G. J., and J. M. Fletcher (1998), Late Miocene Pleistocene extensional faulting, northern Gulf of California, Mexico and Salton Trough, California, *Int. Geol. Rev.*, *40*, 219–244.

Bennett, R. A., W. Rodi, and R. E. Reilinger (1996), Global Positioning System constraints on fault slip rates in Southern California and northern Baja, Mexico, *J. Geophys. Res.*, *101*, 21,943–21,960, doi:10.1029/96JB02488.

Bennett, S. E., and M. E. Oskin (2014), Oblique rifting ruptures continents: Example from the Gulf of California shear zone, *Geology*, *42*(3), 215–218, doi:10.1130/G34904.1.

Bialas, R. W., and W. R. Buck (2009), How sediment promotes narrow rifting: Application to the Gulf of California, *Tectonics*, *28*, TC4014, doi:10.1029/2008TC002394.

Brothers, D., D. Kilb, K. Luttrell, N. Driscoll, and G. Kent (2011), Loading of the San Andreas fault by flood-induced rupture of faults beneath the Salton Sea, *Nat. Geosci.*, *4*, 486–492, doi:10.1038/ngeo1184.

Brothers, D. S., N. W. Driscoll, G. M. Kent, A. J. Harding, J. M. Babcock, and R. L. Baskin (2009), Tectonic evolution of the Salton Sea inferred from seismic reflection data, *Nat. Geosci.*, *2*, 581–584, doi:10.1038/ngeo590.

Brune, S., C. Heine, M. Pérez-Gussinyé, and S. V. Sobolev (2014), Rift migration explains continental margin asymmetry and crustal hyper-extension, *Nat. Commun.*, *5*, 4014, doi:10.1038/ncomms5014.

Christensen, N. I., and W. D. Mooney (1995), Seismic velocity structure and composition of the continental crust: A global view, *J. Geophys. Res.*, *100*, 9761–9788, doi:10.1029/95JB00259.

Dorsey, R. J. (2010), Sedimentation and crustal recycling along an active oblique rift margin Salton Trough and northern Gulf of California, *Geology*, *38*, 443–446, doi:10.1130/G30698.1.

Dorsey, R. J., and G. Lazear (2013), A post-6 Ma sediment budget for the Colorado River, *Geosphere*, *9*, 781–791, doi:10.1130/GES00784.1.

Dorsey, R. J., A. Fluette, K. McDougall, B. A. Housen, S. U. Janecke, G. J. Axen, and C. R. Shirvell (2007), Chronology of Miocene-Pliocene deposits at Split Mountain Gorge, Southern California: A record of regional tectonics and Colorado River evolution, *Geology*, *35*, 57–60.

Elders, W. A., R. W. Rex, T. Meidav, P. T. Robinson, and S. Bieler (1972), Crustal spreading in Southern California, *Science*, *178*, 15–24.

Fuis, G. S., W. M. Mooney, J. H. Healy, G. A. McMechan, and W. J. Lutter (1984), A seismic refraction survey of the Imperial Valley region, California, *J. Geophys. Res.*, *89*, 1165–1189, doi:10.1029/JB089iB02p01165.

González-Escobar, M., C. Aguilar-Campos, F. Suárez-Vidal, and A. Martín-Barajas (2009), Geometry of the Wagner basin, upper Gulf of California based on seismic reflections, *Int. Geol. Rev.*, *51*(2), 133–144.

González-Escobar, M., C. I. Pérez-Tinajero, F. Suarez-Vidal, and A. González-Fernández (2013), Structural characteristics of the Altar Basin, Northwest Sonora, Mexico, *Int. Geol. Rev.*, *55*, 322–336, doi:10.1080/00206814.2012.708981.

Gonzalez-Fernandez, A., J. J. Danobeitia, L. A. Delgado-Argote, F. Michaud, D. Cordoba, and R. Bartolome (2005), Mode of extension and rifting history of upper Tiburon and upper Delfin basins, northern Gulf of California, *J. Geophys. Res.*, *110*, B01313, doi:10.1029/2003JB002941.

Hauksson, E. (2000), Crustal structure and seismicity distribution adjacent to the Pacific and North America plate boundary in Southern California, *J. Geophys. Res.*, *105*, 13,875–13,903, doi:10.1029/2000JB900016.

Hauksson, E., W. Yang, and P. M. Shearer (2012), Waveform relocated earthquake catalog for Southern California (1981 to June 2011), *Bull. Seismol. Soc. Am.*, *102*, 2239–2244, doi:10.1785/0120120010.

Herzig, C. T., J. M. Mehegan, and C. E. Stelting (1988), Lithostratigraphy of the State 2-14 borehole: Salton Sea Scientific Drilling Project, *J. Geophys. Res.*, *93*, 12,969–12,980, doi:10.1029/JB093iB11p12969.

Holbrook, W. S., and P. B. Kelemen (1993), Large igneous province on the United States Atlantic margin and implications for magmatism during continental breakup, *Nature*, *364*, 433–436.

Hole, J. A. (1992), Nonlinear high-resolution three-dimensional seismic travel time tomography. *J. Geophys. Res.*, *97*, 6553-6562. DOI:10.1029/92JB00235.

Hole, J. A., and B. C. Zelt (1995), 3-D finite-difference reflection traveltimes, *Geophys. J. Int.*, *121*(2), 427–434.

Hopper, J. R., T. Funck, B. E. Tucholke, H. C. Larsen, W. S. Holbrook, K. E. Louden, D. Shillington, and H. Lau (2004), Continental breakup and onset of ultraslow seafloor spreading off Flemish Cap on the Newfoundland rifted margin, *Geology*, *32*, 93–96.

Huismans, R. S., and C. Beaumont (2014), Rifted continental margins: The case for depth-dependent extension, *Earth Planet. Sci. Lett.*, *407*, 148–162, doi:10.1016/j.epsl.2014.09.032.

Janecke, S. U., R. J. Dorsey, D. Forand, A. N. Steely, S. M. Kirby, A. T. Lutz, B. A. Housen, B. Belgarde, V. E. Langenheim, and T. M. Rittenour (2010), High geologic slip rates since early Pleistocene initiation of the San Jacinto and San Felipe Fault zones in the San Andreas Fault system, Southern California, USA, *Geol. Soc. Am. Spec. Pap.*, *475*, 1–48, doi:10.1130/2010.2475.

Kairouz, M. E. (2005), Geology of the Whale Peak region of the Vallecito Mountains: Emphasis on the kinematics and timing of the West Salton detachment fault, Southern California, MS thesis, Univ. of Calif., Los Angeles.

Kell, A. M., V. J. Sahakian, A. J. Harding, G. M. Kent, and N. W. Driscoll (2012), Shallow sediment and upper crustal structure beneath the Salton Sea as imaged by active source marine seismic refraction in conjunction with the Salton Seismic Imaging Project, Abstract T51B-2578 presented at 2012 Fall Meeting, AGU, San Francisco, Calif., 3–7 Dec.

Kirby, S. M., S. U. Janecke, R. J. Dorsey, B. A. Housen, V. E. Langenheim, K. A. McDougall, and A. N. Steely (2007), Pleistocene Brawley and Ocotillo Formations: Evidence for initial strike-slip deformation along the San Felipe and San Jacinto Fault zones, Southern California, *J. Geol.*, *115*, 43–62.

Kohler, M. D., H. Magistrale, and R. W. Clayton (2003), Mantle heterogeneities and the SCEC reference three-dimensional seismic velocity model version 3, *Bull. Seismol. Soc. Am.*, *93*(2), 757–774.

Kohler, W. M., and G. S. Fuis (1986), Travel-time, time-term, and basement depth maps for the Imperial Valley region, California, from explosions, *Bull. Seismol. Soc. Am.*, *76*(5), 1289–1303.

Lachenbruch, A. H., J. H. Sass, and S. P. Galanis Jr. (1985), Heat flow in southernmost California and the origin of the Salton Trough, *J. Geophys. Res.*, *90*, 6709–6736, doi:10.1029/JB090iB08p06709.

Larkin, S. P., A. Levander, D. Okaya, and J. A. Goff (1996), A deterministic and stochastic velocity model for Salton Trough/Basin and Range transition zone and constraints on magmatism during rifting, *J. Geophys. Res.*, *101*, 27,883–27,897, doi:10.1029/96JB02535.

Larsen, S., and R. Reilinger (1991), Age constraints for the present fault configuration in the Imperial Valley, California: Evidence for north-westward propagation of the Gulf of California rift system, *J. Geophys. Res.*, *96*, 10,339–10,346, doi:10.1029/91JB00618.

Larson, R. L., H. W. Menard, and S. M. Smith (1968), Gulf of California: A result of ocean-floor spreading and transform faulting, *Science*, *161*, 781–784.

Lee, E., P. Chen, T. H. Jordan, P. B. Maechling, M. A. M. Denolle, and G. C. Beroza (2014), Full-3-D tomography for crustal structure in Southern California based on the scattering-integral and the adjoint-wavefield methods, *J. Geophys. Res. Solid Earth*, *119*, 6421–6451, doi:10.1002/2014JB011346.

Lekic, V., S. W. French, and K. M. Fischer (2011), Lithospheric thinning beneath rifted regions of Southern California, *Science*, *334*, 783–787, doi:10.1126/science.1208898.

Lin, G. (2013), Three-dimensional seismic velocity structure and precise earthquake relocations in the Salton Trough, Southern California, *Bull. Seismol. Soc. Am.*, *103*(5), 2694–2708, doi:10.1785/0120120286.

Lin, G., P. M. Shearer, E. Hauksson, and C. H. Thurber (2007), A three-dimensional crust seismic velocity model for Southern California from a composite event method, *J. Geophys. Res.*, *112*, B11306, doi:10.1029/2007JB004977.

Lin, G., C. H. Thurber, H. Zhang, E. Hauksson, P. M. Shearer, F. Waldhauser, T. M. Brocher, and J. Hardebeck (2010), A California statewide three-dimensional seismic velocity model from both absolute and differential times, *Bull. Seismol. Soc. Am.*, *100*, 225–240, doi:10.1785/0120090028.

Lizarralde, D., et al. (2007), Variation in styles of rifting in the Gulf of California, *Nature*, *448*, 466–469, doi:10.1038/nature06035.

Lonsdale, P. (1989), Geology and tectonic history of the Gulf of California, in *The Eastern Pacific Ocean and Hawaii*, *The Geol. of North Am.*, vol. N, edited by E. L. Winterer, D. M. Hussong, and R. W. Decker, pp. 499–521, Geol. Soc. Am, Boulder, Colo.

Lovely, P., J. H. Shaw, Q. Liu, and J. Tromp (2006), A structural Vp model of the Salton Trough, California, and its implications for seismic hazard, *Bull. Seismol. Soc. Am.*, *96*, 1882–1896.

Magistrale, H., H. Kanamori, and C. Jones (1992), Forward and inverse three-dimensional *P* wave velocity models of the Southern California crust, *J. Geophys. Res.*, *97*, 14,115–14,135, doi:10.1029/92JB00494.

Magistrale, H., S. Day, R. W. Clayton, and R. Graves (2000), The SCEC Southern California reference three-dimensional seismic velocity model version 2, *Bull. Seismol. Soc. Am.*, *90*, S65–S76.

Martin-Barajas, A., M. Gonzalez-Escobar, J. M. Fletcher, M. Pacheco, M. Oskin, and R. Dorsey (2013), Thick deltaic sedimentation and detachment faulting delay the onset of continental rupture in the Northern Gulf of California: Analysis of seismic reflection profiles, *Tectonics*, *32*, 1294–1311, doi:10.1002/tect20063.

McMechan, G. A., and W. D. Mooney (1980), Asymptotic ray theory and synthetic seismogram for laterally varying structures: Theory and application to the Imperial Valley, California, *Bull. Seismol. Soc. Am.*, *70*, 2021–2035.

Muffler, L. J. P., and B. R. Doe (1968), Composition and mean age of detritus of the Colorado River delta in the Salton Trough, southeastern California, *J. Sediment. Petrol.*, *38*, 384–399.

Onderdonk, N. W., S. F. McGill, and T. K. Rockwell (2015), Short-term variations in slip rate and size of prehistoric earthquakes during the past 2000 years on the northern San Jacinto Fault zone, a major plate-boundary structure in Southern California, *Lithosphere*, *7*(3), 211–234, doi:10.1130/L393.1.

Oskin, M., and J. Stock (2003), Miocene to recent Pacific-North America plate motion and opening of the Upper Delfin Basin, northern Gulf of California, Mexico, *Geol. Soc. Am. Bull.*, *115*, 1173–1190.

Oskin, M., J. Stock, and A. Martin-Barajas (2001), Rapid localization of Pacific-North America plate boundary motion in the Gulf of California, *Geology*, *29*, 459–462.

Pacheco, M., A. Martin-Barajas, W. Elders, J. M. Espinosa-Cardena, J. Helenes, and A. Segura (2006), Stratigraphy and structure of the Altar basin of NW Sonora: Implications for the history of the Colorado River delta and the Salton Trough, *Rev. Mex. Cienc. Geol.*, *23*, 1–22.

Parsons, T., and J. McCarthy (1996), Crustal and upper mantle velocity structure of the Salton Trough, southeast California, *Tectonics*, *15*, 456–471, doi:10.1029/95TC02616.

Parsons, T., J. McCarthy, W. M. Kohler, C. J. Ammon, H. M. Benz, J. A. Hole, and E. E. Criley (1996), Crustal structure of the Colorado Plateau, Arizona: Application of new long-offset seismic data analysis techniques, *J. Geophys. Res.*, *101*, 11,173–11,194, doi:10.1029/95JB03742.

Perry, H. K. C., C. Jaupart, J. C. Mareschal, and N. M. Shapiro (2006), Upper mantle velocity-temperature conversion and composition determined from seismic refraction and heat flow, *J. Geophys. Res.*, *111*, B07301, doi:10.1029/2005JB003921.

Persaud, P., J. M. Stock, M. S. Steckler, A. Martin-Barajas, J. B. Diebold, A. Gonzalez-Fernandez, and G. S. Mountain (2003), Active deformation and shallow structure of the Wagner, Consag, and Delfin Basins, northern Gulf of California, Mexico, *J. Geophys. Res.*, *108*(B7), 2355, doi:10.1029/2002JB001937.

Richards-Dinger, K. B., and P. M. Shearer (1997), Estimating crustal thickness in Southern California by stacking *PmP* arrivals, *J. Geophys. Res.*, *102*, 15,211–15,224, doi:10.1029/97JB00883.

Robinson, P. T., W. A. Elders, and L. J. P. Muffler (1976), Quaternary volcanism in Salton Sea geothermal field, Imperial Valley, California, *Geol. Soc. Am. Bull.*, *87*, 347–360.

Rose, E. J., et al. (2013), Borehole-explosion and air-gun data acquired in the 2011 Salton Seismic Imaging Project (SSIP), Southern California—Description of the survey, *U.S. Geol. Surv. Open-File Rep. 2013-1172*, 83pp., doi:10.3133/ofr20131172.

Sahakian, V., A. Kell, A. Harding, N. Driscoll, and G. Kent (2016), Geophysical evidence for a San Andreas subparallel transtensional fault along the northeastern shore of the Salton Sea, *Bull. Seismol. Soc. Am.*, doi:10.1785/0120150350.

Savage, B., and Y. Wang (2012), Integrated model for the crustal structure in the Gulf of California extensional province, *Bull. Seismol. Soc. Am.*, *102*, 878–885, doi:10.1785/0120110196.

Schmandt, B., and E. Humphreys (2010), Complex subduction and small-scale convection revealed by body-wave tomography of the western United States upper mantle, *Earth Planet. Sci. Lett.*, *297*, 435–445.

Schmitt, A. K., and J. B. Hulen (2008), Buried rhyolites within the active, high-temperature Salton Sea geothermal system, *J. Volcanol. Geotherm. Res.*, *178*(4), 708–718.

Schmitt, A. K., and J. A. Vazquez (2006), Alteration and remelting of nascent oceanic crust during continental rupture: Evidence from zircon geochemistry of rhyolites and xenoliths from the Salton Trough, California, *Earth Planet. Sci. Lett.*, *252*, 260–274.

Schmitt, A. K., A. Martín, B. Weber, D. F. Stockli, H. Zou, and C.-C. Shen (2013), Oceanic magmatism in sedimentary basins of the northern Gulf of California rift, *Geol. Soc. Am. Bull.*, *125*(11–12), 1833–1850, doi:10.1130/B30787.1.

Shirvell, C. R., D. F. Stockli, G. J. Axen, and M. Grove (2009), Miocene-Pliocene exhumation along the west Salton detachment fault, Southern California, from (U-Th)/He thermochronometry of apatite and zircon, *Tectonics*, *28*, TC2006, doi:10.1029/2007TC002172.

Steely, A. N., S. U. Janecke, R. J. Dorsey, and G. J. Axen (2009), Early Pleistocene initiation of the San Felipe fault zone, SW Salton Trough, during reorganization of the San Andreas Fault system, *Geol. Soc. Am. Bull.*, *121*, 663–687, doi:10.1130/B26239.

Stock, J. M. (2000), Relation of the Puertecitos volcanic province, Baja California, Mexico, to development of the plate boundary in the Gulf of California, in *Cenozoic Tectonics and Volcanism of Mexico*, *Spec. Pap.*, vol. 334, edited by H. Delgado-Granados, G. Aguirre-Diaz, and J. M. Stock, pp. 143–156 , Geol. Soc. Am.

Stock, J. M., and K. V. Hodges (1989), Pre-Pliocene extension around the Gulf of California and the transfer of Baja California to the Pacific Plate, *Tectonics*, *8*, 99–115, doi:10.1029/TC008i001p00099.

Tape, C., Q. Liu, A. Maggi, and J. Tromp (2009), Adjoint tomography of the Southern California crust, *Science*, *325*, 988–992, doi:10.1126/science.1175298.

Vidale, J. E. (1990), Finite difference calculation of travel times in three dimensions, *Geophysics*, *55*, 521–526.
White, R., and D. McKenzie (1989), Magmatism at rift zones: The generation of volcanic continental margins and flood basalts, *J. Geophys. Res.*, *94*, 7685–7729, doi:10.1029/JB094iB06p07685.
Whitmarsh, R. B., G. Manatschal, and T. A. Minshull (2001), Evolution of magma-poor continental margins from rifting to seafloor spreading, *Nature*, *413*, 150–154.
Zelt, B. C., R. M. Ellis, R. M. Clowes, and J. A. Hole (1996), Inversion of three-dimensional wide-angle seismic data from the southwestern Canadian Cordillera, *J. Geophys. Res.*, *101*, 8503–8529, doi:10.1029/95JB02807.
Zelt, C. A. (1999), Modelling strategies and model assessment for wide-angle seismic traveltime data, *Geophys. J. Int.*, *139*, 183–204.
Zhao, D., H. Kanamori, and E. Humphreys (1996), Simultaneous inversion of local and teleseismic data for the crust and mantle structure of Southern California, *Phys. Earth Planet. Inter.*, *93*, 191–214.